Sensors and Actuators A 255 (2017) 10–20

Contents lists available at ScienceDirect

Sensors and Actuators A: Physical

journal homepage: www.elsevier.com/locate/sna

Electric field enhanced 3D scalable low-voltage nano-spike electroporation system

Kashif Riaz [a,d], Siu-Fung Leung [b], Zhiyong Fan [b], Yi-Kuen Lee [a,c,*]

[a] Department of Mechanical & Aerospace Engineering, Hong Kong University of Science and Technology, Clear Water Bay, Kowloon, Hong Kong Special Administrative Region
[b] Department of Electronic & Computer Engineering, Hong Kong University of Science and Technology, Clear Water Bay, Kowloon, Hong Kong Special Administrative Region
[c] Division of Biomedical Engineering, Hong Kong University of Science and Technology, Clear Water Bay, Kowloon, Hong Kong Special Administrative Region
[d] Department of Electrical Engineering, Information Technology University (ITU), Lahore, Pakistan

ARTICLE INFO

Article history:
Received 26 June 2016
Received in revised form
14 December 2016
Accepted 22 December 2016
Available online 28 December 2016

Keywords:
Nano-spike electroporation chips
Scalable
Electroporation
Efficient molecules delivery
High cell viabilities
Electric field enhancement
High-aspect-ratio

ABSTRACT

Electroporation (EP) is one of the most widely used methods for the introduction of bio-molecules into the cells due to its high efficiencies, simplicity, and safety. Previous macro- and micro-scale EP systems suffer from drawbacks such as costly and time-consuming fabrication processes, high voltage operation causes undesirable electrochemical reactions, low cell viabilities, and electrode degradation. In this paper, we presented a low-cost three-dimensional (3D) scalable nano-spike electroporation system for efficient molecules delivery with high cell viabilities at low applied voltages. Arrays of 3D Aluminum (Al) nano-spikes (NSPs) were fabricated through scalable, reproducible and cost effective electrochemical anodization and etching processes. Due to scalability of the fabrication process, 3D NSPs were fabricated on chips as well as at the wafer level for large scale processing. 3D nano-spike electroporation (NSP-EP) chips were capable of handling small cell populations (100–500) while NSP-EP wafers can handle large cell populations (10^4–10^5). Electroporation at low voltages is obtained due to electric field enhancement at high-aspect-ratio NSPs. With same electric field strength, high EP efficiencies η_{EP} and cell viability ϕ_{cell} (>93 ± 6%) were obtained at more than ten times lower voltages (2 V) on NSP-EP chips as compared to planar electroporation (PEP) devices without NSPs. By optimizing electric pulse parameters and nano-spikes dimensions, NSP-EP chip performance was enhanced by minimizing undesirable electrochemical reactions and electrolysis that were observed on PEP devices due to high voltage operations.

1. Introduction

The introduction of exogenous molecules such as proteins, drugs and genetic material with high efficiency and viability through the cell membrane is a critical step in analytical and diagnostic microsystems [1–4]. Different approaches have been used to transfer these molecules, such as chemical, biological or physical methods. Chemical and biological methods are often limited due to low efficiency, toxicity and safety concerns [5–7]. Due to the simplicity, safety and high efficiency; physical methods have been adopted to directly deliver the molecules and agents into the cells [5–8]. The most common and widely used physical method is electroporation (EP) due to its simplicity, low cost, safety, efficiency, fast delivery, and applicability to diverse cell types and sizes. EP uses electric fields to induce reversible nanopores expansion in the cell membrane so that it becomes permeable to exogenous molecules [9–11]. Besides these advantages, several disadvantages are associated with the conventional electroporation system (cuvette type) due to high voltage requirements to achieve critical electric field for EP (E_{EP}) [12–14]. Due to high voltage operations, conventional EP system undergoes metal ion dissolution [12,13], local pH variation [12,13], joule heating [12,14], local pH variation [12,13], distorted electric field [12], gas and bubble generation [15], sample contamination due to electrode degradation and irreversible electroporation resulted in low EP efficiency electroporation and low cell viability [12–15]. In addition, conventional EP system requires bulky and costly high voltage pulse generators [16], large volumes of sample solutions, expensive reagents, and cells.

Micro-scale EP is getting more attention as compared to conventional bulky EP systems due to several advantages, such as

* Corresponding author at: Department of Mechanical & Aerospace Engineering, Hong Kong University of Science and Technology, Clear Water Bay, Kowloon, Hong Kong Special Administrative Region.
E-mail address: meyklee@ust.hk (Y.-K. Lee).

http://dx.doi.org/10.1016/j.sna.2016.12.022
0924-4247/

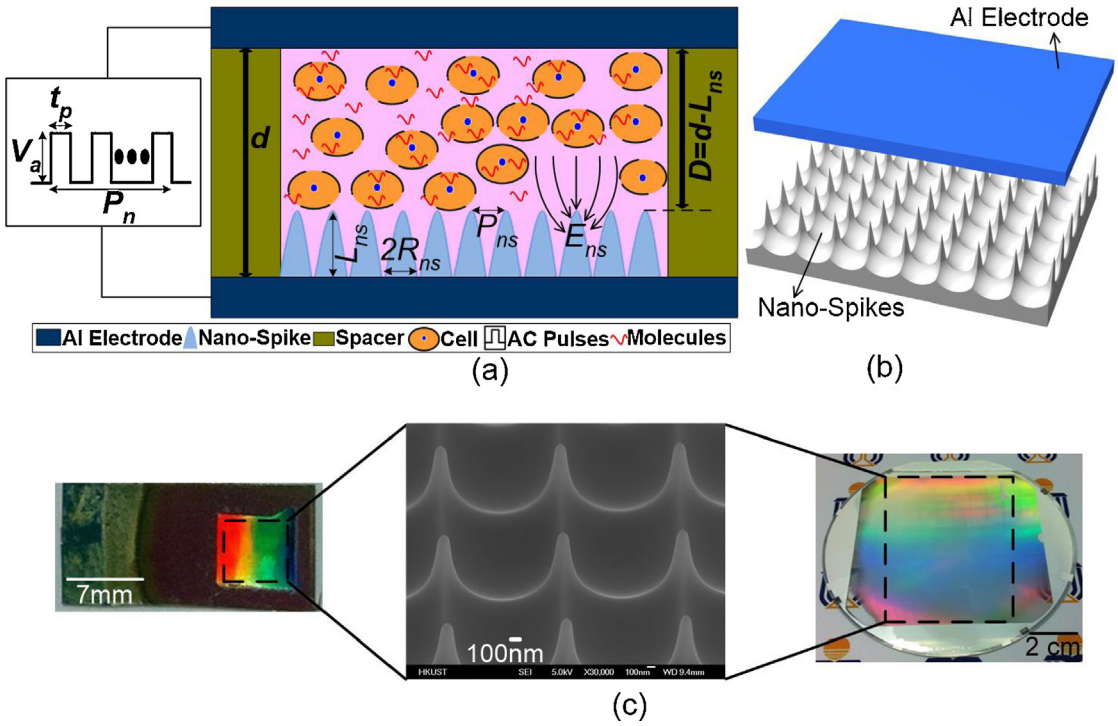

Fig. 1. Illustration of Nano-Spike Electroporation (NSP-EP) chip, (a) 2D schematic of NSP-EP chip shows electric field enhancement at nano-spikes (NSPs) due to high aspect ratio λ (=L_{ns}/R_{ns}), (b) 3D schematic of NSP-EP chip and (c) SEM image of arrays of NSPs fabricated on an Aluminum (Al) foil of area of 49 mm^2 and a 4-inch glass wafer.

high efficiency, spatiotemporal control, in situ visualization, real-time monitoring, rapid protocol optimization and single-cell EP [12,14,15,17–20]. Critical electric field E_{EP} was achieved at much lower voltages as compare to conventional EP either by placing electrodes in close proximity (reducing the distance between electrodes) or focusing electric field through small constriction segments and structures in micro-channels or micro-chambers [5,12,14,15]. Micro electrodes in close proximity were placed either in micro-channel or micro-chamber in parallel plate or coplanar configuration [12,14,18,21]. The depth of these 2D electrodes was usually smaller than the size of the cells, so small portion of cells was exposed to an electric field which resulted in electroporation of small sample volume at once [22]. The thin metal layers of these electrodes were not stable and had tendency to decay due to undesirable electrochemical reactions such as gas and bubble generation [15,23]. These issues of 2D electrodes were addressed by fabrication various types of 3D electrodes [14,22]. But the fabrication of these 3D electrodes usually involves complex, time consuming and costly steps [24,25]. Also the separation distance between electrodes in micro-devices is limited by cell sizes [26].

Microelectrodes in close proximity usually suffer from degradation due to electrolysis depending on applied pulse parameters [15,27]. Pulses of high amplitude, duration and number result in the electrolysis of water which causes bubble and gas formation. Due to these undesirable electrochemical reactions, cell viabilities were dropped by sample contamination, pressure exertion by bubbles and arcing [23,28–30]. These problems can be minimized by lowering the average electrical current through increasing the resistance between the electrodes [14]. Constriction segments or structures in the channels were employed so that maximum potential drop was across the cell membrane trapped in these structures instead of in the vicinity of the electrode [14,17,19,31–33]. Although electrode degradation can be minimized but the fabrication of such structures and segments involves complex and costly manufacturing steps [14]. Besides, these constriction segments and structures in micro-channels require expensive equipment and suffer from channel blocking by cells or bubbles [14,15,27,34,35]. The average electric current can also be reduced by applying AC pulses with low amplitude and shorter duration, but pulse parameters should be optimized to achieve high efficiencies and cell viabilities in addition to minimizing electrochemical reactions [15,34,36,37].

Nanostructures such as nano-tubes, nano-wires, nano-pillars, and nano-straws electrodes fabricated with different materials have been used recently for EP [38–48]. EP on these electrodes has been achieved at reduced voltages as compared to planar electrodes without nano-structures [39–48]. EP at reduced voltages has been performed due to high-aspect-ratio nano-structures which resulted in the enhanced electric field. Rojas-Chapana et al. used multi-walled carbon nano-tubes (MWCNT) for microwave based electroporation of gram-negative bacteria [39]. They specify the "lightening rod effect" for electric field localization at the CNT tips. Raffa et al. used MWCNT to achieve reversible electroporation at the lower electric field of 0.05 kV/cm with the efficiency of ~80% as compared to macro plate electrodes (0.5–100 kV/cm) [41]. Chen et al. fabricated ITO electrodes with a gap of 500 nm to localized electric field for single cell and achieved cell viabilities of 80–95% at applied voltages of 12 V [43]. Xie et al. used alumina nano-straw electroporation system and achieved efficiency of 95% at 20 V [46].

Although the nano-structured electrodes enabled the enhanced EP at reduced voltages as compared to planar electrodes, the applied voltages used in the previous works are still in the range of tens of volts to achieve EP with high efficiency and cell viability [39–48] (see supplementary information (SI), Table S1). This is highly undesirable in portable lab-on-chip (LOC), micro total analysis system (μTAS) and smartphone-based systems with limited power source [1,2,4,49]. One of the bottlenecks in the integration of nano-structures on the microsystems is the difficulties in handling and positioning the nano-structures at the exact desired location to fabricate reproducible, periodic and uniform nano-structures [4]. Furthermore, the fabrication techniques employed in the fabrication of these nano-structures using conventional techniques are complex, costly, time consuming and non-reproducible [4]. It is

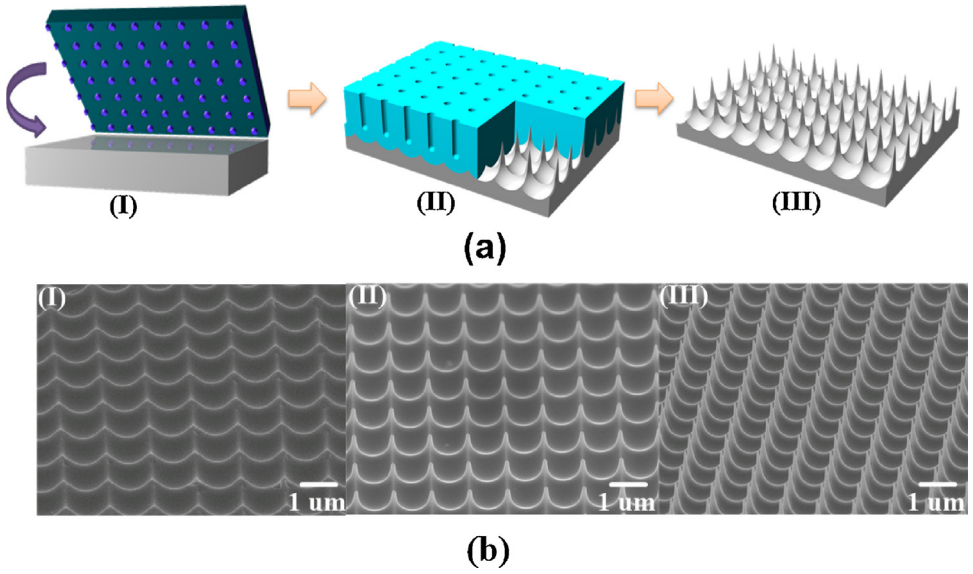

Fig. 2. (a) Schematics of 3D periodic nano-spike arrays fabrication process, (I) the cleaned Al foil substrate was imprinted using a silicon mold with squarely patterned pillars resulted in periodic nano-holes on substrate, (II) imprinted substrate was anodized and then etched in a mixture of phosphoric acid and chromic acid for the fabrication of nano-spike arrays, and (III) fabricated 3D nano-spike arrays on substrate. (b) SEM images of nano-spike electrodes with different lengths L_{ns} of, (I) 350 nm, (II) 750 nm, (III) 1100 nm.

highly desirable to establish simple, inexpensive, reliable and scalable fabrication techniques for fabrication of reproducible, periodic and uniform nano-structures to be used in their integration on microsystem and potential mass production [1,2,4,49].

In this work, we present a 3D scalable nano-spike based EP system which utilized highly ordered self-aligned 3D Aluminum (Al) nano-spike (NSP) arrays fabricated through electrochemical anodization and etching processes. Due to their simplicity, low cost and scalability, electrochemical anodization and etching processes have been used recently for the fabrication of self-aligned highly ordered 3D nano-structures [50]. Nano-structures fabricated through electrochemical anodization and etching processes using anodic alumina membrane(AAM) as template showed great potential applications in the field of magnetism, electronics, optoelectronic, photovoltaic, medical, and biology [50–55]. Alumina is recognized as bio-compatible material and used in hip arthroplasty [56], tissue engineering especially for skin replacement [57], bone implant [58], and cell culture and proliferation [59].

We fabricated a 3D scalable nano-spike based EP system which utilized nano-spike electroporation (NSP-EP) chips and a computer-controlled electric pulse generator (Fig. 1) for efficient intracellular molecules delivery with high cell viabilities at low pulse amplitudes and durations. NSP-EP chips have highly-ordered 3D Al NSP arrays with controllable dimensions such as length, L_{ns}, base radius, R_{ns}, and pitch, P_{ns} (spike to spike distance). These NSPs were fabricated on low-cost commercial Al foils through simple, scalable, reproducible and cost effective electrochemical anodization and etching processes (Fig. 2). Highly-ordered 3D NSPs with high-aspect-ratios, λ ($=L_{ns}/R_{ns}$) have been fabricated (Fig. 2). The electric field has been localized at NSPs due to high λ with an enhancement factor α as compared to planar EP devices (PEP) (Fig. 3). NSP-EP chips have achieved high EP efficiencies η_{EP} and cell viability Φ_{cell} at more than ten times reduced pulse amplitudes through localized electric field E_{ns} as compared to the planar EP devices (PEP) without NSPs (Fig. 4). The employment of electrochemical fabrication process, optimized AC electric pulses with low amplitudes and short durations minimize undesirable electrochemical reactions, such as gas and bubble generation and electrolysis of cells on NSP-EP chips (Fig. 4). Due to scalability of fabrication process, highly ordered 3D NSPs were fabricated on small chips as well as on wafers to process samples for microsystems as well as for high throughput applications (Fig. 1).

2. Material and methods

2.1. 3D nano-spike arrays fabrication

Process steps involved in the fabrication of highly-ordered 3D Al NSP arrays are as follows [51]. First of all, low-cost commercial Al foils (99.99% Alfa Aesar, MA, USA) with a thickness of *ca* 250 μm were cut into 2×1 cm^2 pieces. These pieces were then cleaned with acetone followed by isopropyl alcohol and deionized (DI) water rinsing. The cleaned pieces were electrochemically polished in a 1:3 (v:v) mixture of perchloric acid and ethanol for 4 min at 5 °C. The electropolished Al foils were imprinted by a silicon stamp to nano-imprint the squarely ordered nanoindentation for location definition of the anodic alumina (AAM) pores (Fig. 2(a)). Al foils had perfect squarely ordered nano-indentation after nano-imprint (Fig. 2(a)). Silicon stamp had squarely patterned pillar with a height of ~200 nm, a diameter of 500 nm and a pitch P_{ns} of 1.2 μm. The substrates were then anodized in a home-built anodization setup in a mixture of citric acid, ethylene glycol, and phosphoric acid. Different anodization conditions were used to achieve different heights of NSPs i.e. the electrolyte voltage was 480 V, while the anodization time was 180. The anodized AAM layer was then etched away in a mixture of phosphoric acid (6%) and chromic acid (1.5%) at 63 °C for 50 min (Fig. 2(b)) to obtain perfectly ordered 3D NSP arrays (Fig. 2(b)). 3D Al NSP electrodes were cleaned with DI water and dried with air.

2.2. NSP-EP chip fabrication

Al foils with a thickness of *ca* 250 μm and area of 2×1 cm^2 were cleaned, and NSPs were fabricated on an area of 7×7 mm^2 using nano-imprinting, electrochemical anodization and etching as discussed in the previous section. Note that this fabrication technique is scalable and it ranges from a small chip to a wafer (Fig. 1(c)). The top electrode was separated from the bottom electrode through a spacer (3 M Orange Polyimide electrical insulation tape) with thickness d of 100 μm (Fig. 1(a)). This spacer not only insulated two

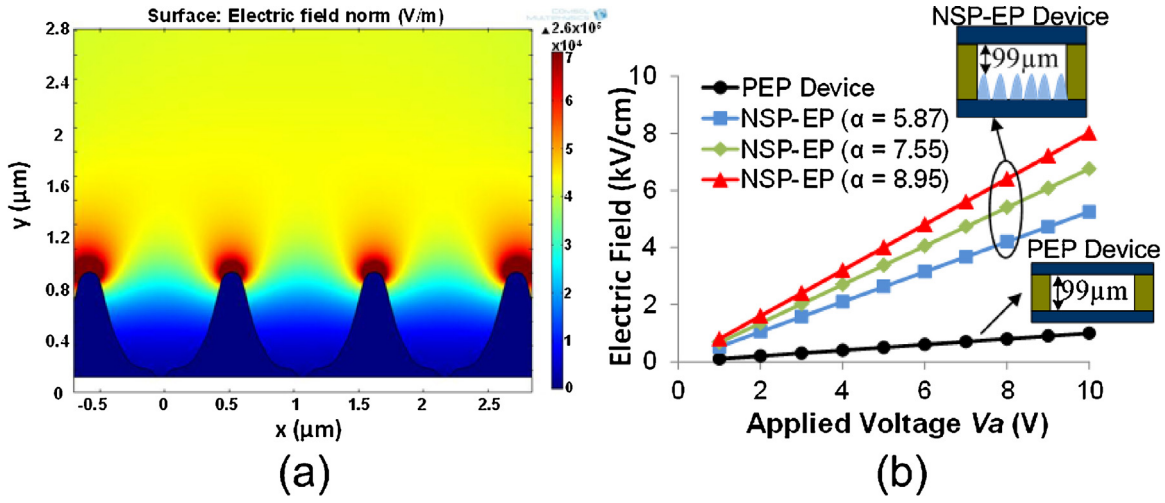

Fig. 3. (a) Numerical simulation of the electric field distribution between nano-spike array electrodes ($\lambda = 2.5$) using COMSOL at applied voltage $V_a = 4$ V. The simulation shows enhanced electric field E_{ns} with enhancement factor α depending on aspect ratio λ of NSPs, (b) Electric field as function of applied voltages V_a for planar electroporation (PEP) device without nano-spikes and NSP-EP devices with different α.

electrodes but also formed a micro-well to inject cell suspension and molecules for EP (Fig. 1(a)-(b)). Before EP experiments, NSP-EP chips were sterilized with 75% ethanol solution, rinsed with DI water and then dried in a 65 °C oven.

2.3. Cell culturing

Human cervical cancer (HeLa) cell line was used in the EP experiments to characterize EP efficiency η_{EP}, cell viability Φ_{cell} and operating conditions of NSP-EP chips. HeLa cells were grown as a monolayer in a 60 mm petri dish in Eagle's minimal essential medium (EMEM) (CCL-2™, ATCC, VA, USA), supplemented with 10% fetal bovine serum (FBS) (ATCC, VA, USA) and 1% Streptomycin/Penicillin (GIBCO®, Invitrogen Inc., USA) at 37 °C and 5% CO_2. To perform EP experiments, HeLa cells were re-suspended in the EP medium (EMEM supplemented with 10% FBS). To get cell suspension, the EMEM medium was vacuumed; cells were washed twice with PBS and the attached cells on petri dish were trypsinized by 0.25% trypsin/EDTA (GIBCO®, Invitrogen Inc., USA) for 3–5 min at 37 °C. The trypsinized cells were centrifuged at 1200 rpm at room temperature for 3 min and concentration of HeLa cells were adjusted to 1×10^5 cells/mL in the cell suspension.

2.4. Experimental setup

The pulsed electric field with adjustable pulse amplitude (V_a), pulse duration (t_p) and pulse number (P_n) was applied to the NSP-EP chips using a PCI 6110 DAQ card (National Instrument, TX, USA) and a Labview program (see SI, Fig. S1). The applied pulse signal variation was ±0.02 V. An Olympus IX70 inverted fluorescent microscope and a QImaging Retiga 1300C digital CCD camera (Burnaby, B.C., Canada) were used for in situ visualization of the cell's response (see SI, Fig. S1). The 100 W mercury lamp with sets of fluorescence filters (excitation by a 515–565 nm bandpass filter and the emission by a 550–655 nm bandpass filter) was used for the optical microscopy of the cells on the NSP-EP chips. Sets of bright field and fluorescent micrographs were acquired by an image capture card. These images have been used to determine the η_{EP} and Φ_{cell} as functions of V_a, t_p and P_n.

2.5. Dual acridine orange/propidium iodide fluorescent staining

Acridine Orange and Propidium Iodide (AO/PI; Sigma, St Louis, MO, USA) dual fluorescent dye staining was used to determine electroporation efficiency η_{EP}. Both Acridine Orange (AO) and Propidium Iodide (PI) are nuclear staining dyes. AO is a membrane permeable dye and stains all cells and emits green fluorescence. PI is membrane impermeable dye which can enter cells membranes with expanded nano-pores and emits red fluorescence. Cells were suspended in EP medium and dual fluorescent AO/PI staining solution containing 0.7 µg/ml AO and 1 µg/ml PI was added. This cell suspension was injected to NSP-EP chips and electric pulses with different V_a, t_P and P_n were applied. Electroporated cells appeared red under fluorescent mode as PI molecules entered the cells through expanded nano-pores and bonded to the DNA/RNA while non-electroporated cells appeared green. Sets of fluorescent micrographs were acquired 5 min after application of electric pulses to allow the entrance of PI dye into cells. The acquired images were processed to determine η_{EP} as a function of different electric pulse parameters. η_{EP} was calculated by counting the cells appeared red under fluorescent mode over the total cells.

2.6. Dual acridine orange/ethidium bromide fluorescent staining

Acridine Orange and Ethidium Bromide (AO/EB; Sigma, St Louis, MO, USA) dual fluorescent dye staining was used to determine cell viabilities Φ_{cell}. Both Acridine Orange (AO) and Ethidium Bromide (EB) are nuclear staining dyes. AO is a membrane permeable dye and stains all cells and emits green fluorescence. EB is membrane impermeable dye which can enter cells with compromised membranes and emits red fluorescence. When cells are stained with dual AO/EB dyes, live cells emit green fluorescence while dead cells exhibit orange-yellow fluorescence due to loss of membrane integrity. To determine Φ_{cell}, cell suspension without AO/EB was injected to NSP-EP chips and electric pulses with different V_a, t_P and P_n were applied. Dual fluorescent AO/EB staining solution containing 0.5 µg/ml AO and 0.5 µg/ml EB was added to cell suspension 5 min after application of electric pulses to avoid false reading from reversibly electroporated cells. Dead cells appeared orange-yellow under fluorescence due to binding of EB dye with DNA/RNA either inside cytoplasm or outside ruptured cell membrane. Sets of fluorescent micrographs were acquired and processed to determine

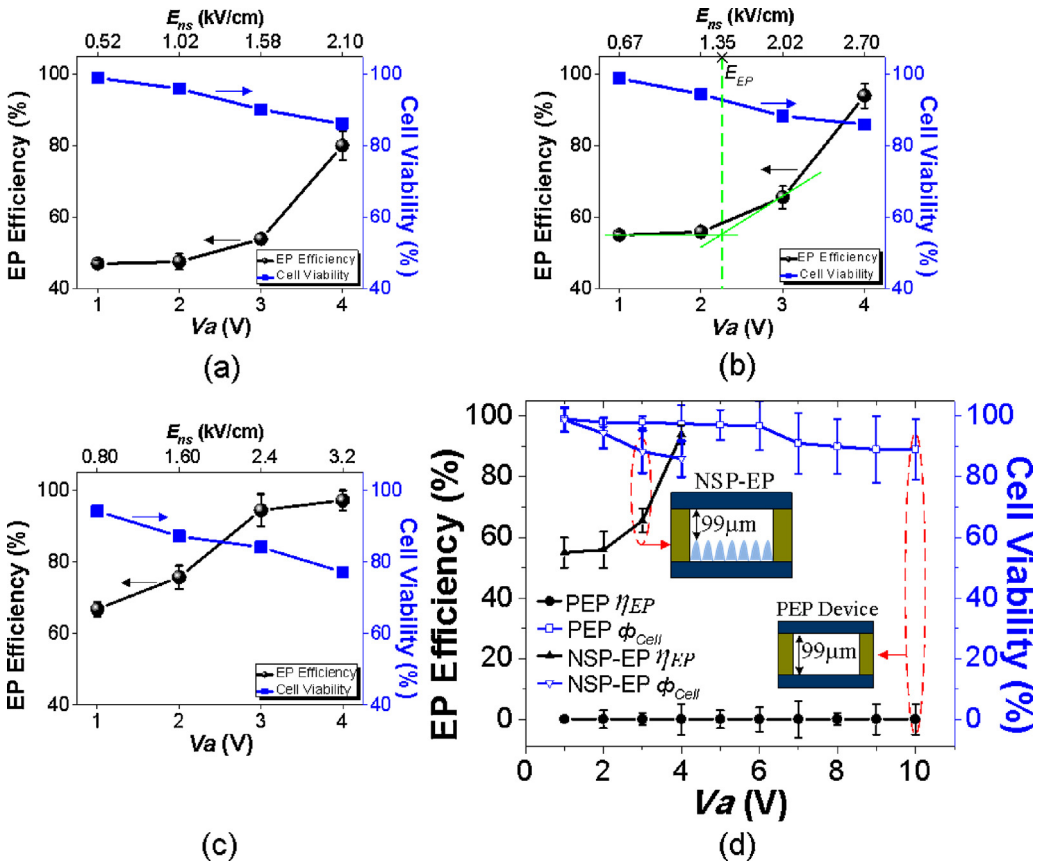

Fig. 4. EP efficiency (η_{EP}) and cell viability (ϕ_{cell}) as a function of applied voltage (V_a) and localized electric field (E_{ns}) with pulse duration t_P of 2 ms on NSP-EP chips with different enhancement factor α, (a) α = 5.87, (b) α = 7.55, and (c) α = 8.95, and (d) η_{EP} and ϕ_{cell} on NSP-EP chip (α = 7.5) and PEP devices as a function of V_a and t_p = 2 ms.

ϕ_{cell} as a function of different electric pulse parameters. ϕ_{cell} was calculated by counting cells appeared orange-yellow under fluorescence over the total cells.

2.7. Statistical analysis

Each data point for η_{EP} and ϕ_{cell} was obtained by analyzing at least 100 cells and each experiment was repeated at least three times. The standard deviation between repeated experiments was shown as error bars.

3. Results and discussion

3.1. 3D NSP-EP system

The 2D and 3D schematics of NSP-EP chip architecture are shown in Fig. 1(a and b). NSP arrays have been fabricated on the Al electrodes with length L_{ns}, base radius R_{ns} and pitch P_{ns}. The top and bottom electrodes are separated by a spacer with a thickness of d (=100 μm) resulted in the formation of micro-well for cell sample and molecules injection (Fig. 1(a)). The gap between tip of the NSPs and the counter electrode of the NSP-EP is defined as D ($=d - L_{ns}$). Due to high aspect ratio λ ($=L_{ns}/R_{ns}$) of NSPs; the applied electric field E_a is enhanced E_{ns} by enhancement factor α. The α, hence enhanced electric field E_{ns} was controlled by controlling dimensions of NSPs. Electric pulses with adjustable pulse amplitudes V_a, pulse durations t_p and pulse number P_n have been applied between two electrodes of NSP-EP chips through a PCI 6110 DAQ card (National Instrument, TX, USA) and a Labview program. Sets of fluorescent micrographs were acquired after EP by an image capture card using an Olympus IX70 inverted fluorescent microscope and a QImaging Retiga 1300C digital CCD camera (Burnaby, B.C., Canada). These acquired images were used to determine the η_{EP} and ϕ_{cell} as functions of electric pulse parameters (V_a, t_p and P_n) and NSPs dimensions. Due to E_{ns}, NSP-EP chips offer the advantage of achieving high η_{EP} and ϕ_{cell} at reduced pulse amplitudes and shorter pulse durations. EP with low pulse amplitudes and shorter pulse durations minimizes undesirable electrochemical reactions such as gas and bubble generation and electrolysis of cells.

3.2. Scalable 3D NSP-EP platform

The 3D NSP array fabrication process is highly scalable and it can range from chip to wafer level. In this work, a typical size of NSP-EP chip is *ca* 7 × 7 mm^2 (Fig. 1(c)). We have successfully fabricated 3D Al NSP arrays on a 4-inch glass wafer (Fig. 1(c)). 3D NSP-EP chips were capable of handling small cell populations (100–500) in μL. The throughput can be scaled up to handle large cell populations (10^4–10^5) on NSP-EP wafers. This simple, low-cost, scalable, reproducible and reliable process is highly attractive for cost-effective portable μ-TAS, LOC, and smartphone-based systems as well as for high throughput and large population applications.

3.3. 3D NSP-EP chips

3D NSP arrays fabrication process for EP was modified from elsewhere [52–55]. It consists of nano-imprint approach in conjunction with two major steps that are scalable electrochemical anodization and etching [60] (Fig. 2(a)). First, clean Al foils were anodized in a mixture of citric acid and ethylene glycol with a DC voltage of 600 V. This anodization step resulted in the formation of anodic alumina membrane (AAM) on an Al substrate (Fig. 2(aII)). The AAM

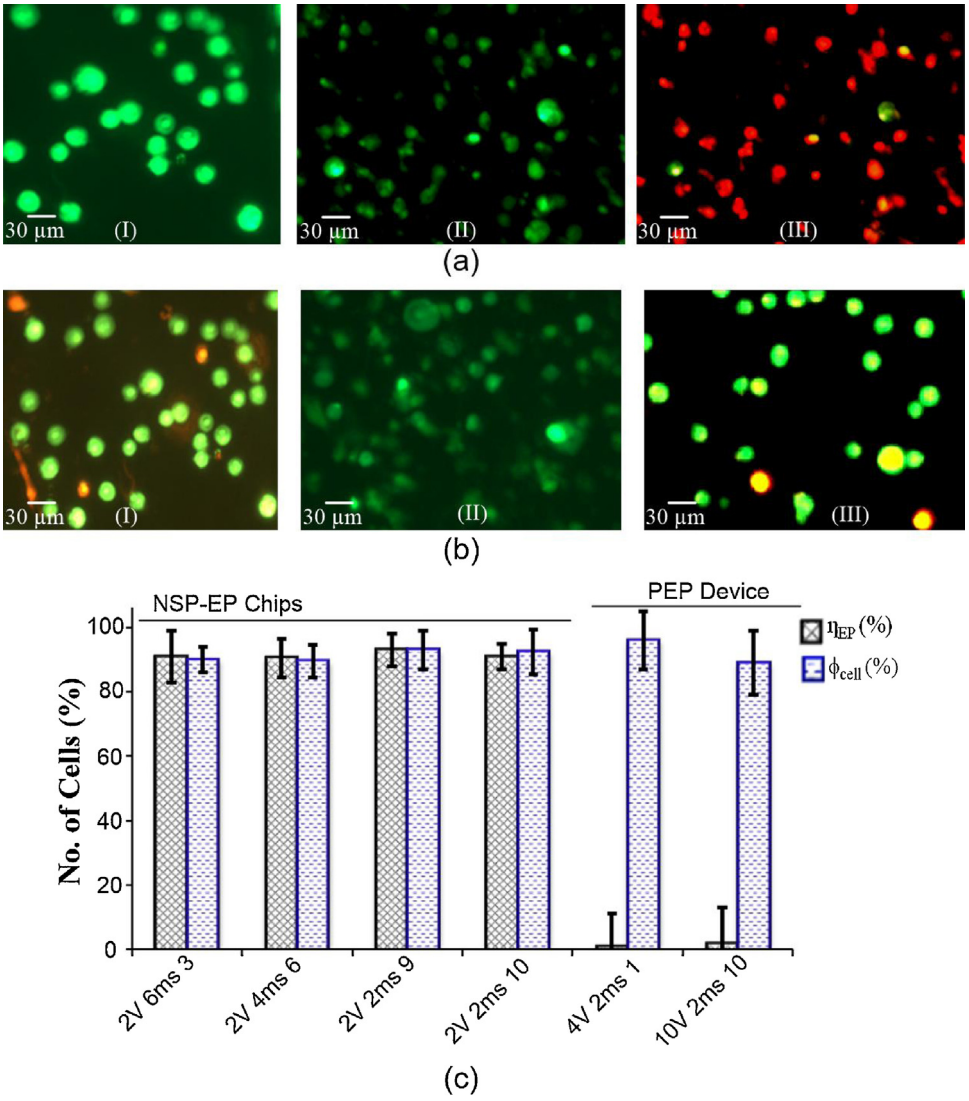

Fig. 5. (a) Fluorescent images of Acridine orange and Propidium iodide dual stained HeLa cells treated on NSP-EP and PEP devices. All viable cells exhibit green fluorescence while electroporated cells exhibit red-orange fluorescence due to pore formation on cell membrane, (I) EP on PEP device at V_a = 5 V and t_P = 2 ms, (II) NSP-EP chips (α = 7.5) before EP, and (III) EP on NSP-EP chips (α = 7.5) at V_a = 2 V, t_P = 2 ms and P_n = 9. (b) Fluorescent images of Acridine orange and Ethidium bromide dual stained HeLa cells treated on NSP-EP and PEP devices. Viable cells exhibit green fluorescence while lysed cells exhibit orange-yellow fluorescence due to loss of membrane integrity, (I) PEP device at V_a = 5 V and t_P = 2 ms, (II) NSP-EP chips (α = 7.5) before EP, (III) NSP-EP chips (α = 7.5) at V_a = 2 V, t_P = 2 ms and P_n = 9. (c) Optimized electric pulse parameter (V_a t_p P_n) to obtain high η_{EP} and ϕ_{cell} on NSP-EP chip (α = 7.5). (For interpretation of the references to colour in this figure legend, the reader is referred to the web version of this article.)

had perfect squarely ordered pores which acted as a template for fabrication of 3D NSP arrays. The AAM layer was then chemically etched away in a mixture of phosphoric and chromic acid resulted in 3D NSP arrays (Fig. 2(aIII)). In this work, citric acid has been used as an electrolyte resulted in better stability [52–55]. Stability of electrolyte was further improved by mixing with ethylene glycol, and the anodization voltage was increased up to 600 V [52–55]. Further details of scalable anodization and etching process steps can be found in the Materials and Methods section.

The length of NSPs can also be precisely controlled by controlling the thickness of AAM and anodization time. The maximum achievable length L_{ns} of NSPs was about ~1100 nm after 360 min anodization. Fig. 2(b) shows sixty degrees tilted SEM images of NSP array electrodes with L_{ns} of 350, 750, and 1100 nm fabricated by 30, 180, and 360 min anodization, respectively and has pitch P_{ns} of 1.2 μm. NSP arrays fabricated using above-mentioned electrochemical process has several advantages including periodicity, self-organization, scalability, reproducibility, and high-aspect-ratio λ.

3.4. Electric field enhancement

Numerical simulations were performed to evaluate the electric field enhancement especially near the tips of NSPs. A commercial finite element method (FEM) package (COMSOL Multiphysics 4.2, COMSOL Ltd., USA) was used for electric field distribution simulation. The profile of NSPs was extracted with the help of extract profiles tool using AFM images of NSPs. The extracted coordinates of NSPs were then exported to COMSOL. Materials were selected for NSP electrodes which are Al in this case. The electrodes were separated by a distance d and space between the electrodes was considered as cell suspension medium. The relative permittivity and conductivity of cell suspension medium were assumed to be 77.4 ± 5% and 1.7 S/m ± 10%, respectively [60]. The fixed potential between the electrodes was used as the boundary condition. The fixed potential between the electrodes was applied by selecting 2D stationary electrostatics physics in COMSOL. Numerical simulations illustrate that the applied electric field E_a is enhanced by

enhancement factor α and enhanced electric field E_{ns} is very strong near tips of NSPs as shown in Fig. 3(a).

In our EP experiments, high η_{EP} and ϕ_{cell} have been achieved at lower pulse amplitudes due to enhanced electric field E_{ns} at NSPs. The electric field at the tips of the NSPs is enhanced due to their high-aspect-ratioλ. The localized enhanced electric field E_{ns} can be estimated using following relation [39,61]:

$$(1) E_{ns} = E_a \times \alpha \times \gamma$$

where α is the electric field enhancement factor, E_a is the applied electric field given by ratio of applied amplitude V_a to distance between electrodes D, γ is the correction factor considering the electrochemical impedance near the fluid-electrode interface [62,63].

Several models have been proposed to estimate α based on the geometries of nanostructures [61]. In our case, by modelling NSP as a hemi-ellipsoid with a length of L_{ns} and a base radius of R_{ns}, the enhancement factor α can be predicted as a function of the NSP aspect-ratioλ [61]:

$$\alpha = \xi^3 / [\{\lambda \ln(\lambda + \xi)\} - \xi] \quad (2)$$

where $\xi = (\lambda^2 - 1)^{1/2}$ and λ is NSP aspect-ratio and given by ratio of L_{ns} to R_{ns}. As previously discussed that NSPs were fabricated with controlled and reproducible dimensions with different λ. It is clear from equation 2 that α is function of λ and increase exponentially withλ. This suggests that very high α can be achieved by selecting appropriate λ as per equation 2. But due to fabrication limitations, we are able to achieve λ up to 3. For NSPs with λ ranging from 2 to 3, α was estimated using equation 2 and it ranged from ~5.9 to 8.9 as shown in Fig. 3(b).

The inter-electrode distance of the planar EP (PEP) device was controlled by a spacer with a thickness of d. On the other hand, the gap between the tip of spikes and the counter electrode of NSP-EP device is the space thickness minus the length of the nano-spike, i.e., $D = d - L_{ns}$. In planar electroporation (PEP) device without NSPs, the applied electric field E_{planar} can be estimated as the ratio of the applied voltage V_a to the distance between electrodes D ($E_{planar} = V_a/D$). In the case of our NSP-EP device, the electric field at the tips of the nano-spike is highly enhanced due to their high aspect ratio of λ with the enhancement factor α. In order to compare electric field for PEP device and NSP-EP devices, same interelectrode distance D (~99 μm) was considered. Localized electric field E_{ns} at NSPs was determined using equation 1. From Fig. 3(b), it is clear that electric field was enhanced at NSP-EP devices as compared to planar electrode devices due to α. This implies that a specific electric field can be achieved at reduced voltages on NSP-EP devices as compared to PEP devices. For example, electric field of 1 kV/cm can be accomplished at 10 V for PEP device, at ~2 V for NSP-EP device with α of 5.87, at ~1.5 V for NSP-EP device with α of 7.55 and at ~1.3 V for NSP-EP device with α of 8.95 (Fig. 3(b)).

For the interelectrode distance of 99 μm and the applied voltage V_a of 4 V, the estimated effective electric field E_a for the PEP device is 0.4 kV/cm which is below critical electric field to induce EP in HeLa cells (1.6 kV/cm for single pulsed EP for HeLa cells) according to our previous study of EP phase diagram for HeLa cells [22]. For the NSP-EP chip, the enhanced electric field E_{ns} for α of 7.55 at 4 V is estimated as 2.7 kV/cm. Therefore, at the same applied voltage of 4 V, the effective electric field of the NSP-EP chip is larger than 1.6 kV/cm. In this paper using NSP-EP chips, we verified that for HeLa cells, we also achieved a critical electric field strength of 1.5–1.6 kV/cm for 2 ms at 2.3 V.

3.5. Electroporation on NSP-EP chips

Cell permeabilization can be induced only when applied electric pulse parameters V_a, t_P and P_n are well above their critical values [22,64]. Transient and localized micro structural changes and nanopore generation in the cell membrane is initiated by the electric field strength which is determined by the pulse amplitude V_a at or above critical value. The pulse duration t_P and number P_n provides the required time for nano-pore growth. The time duration and density of nanopores on cell membranes highly depend on V_a, t_P, and P_n. It is highly desirable to optimize these electric pulse parameters to achieve high η_{EP} and ϕ_{cell} simultaneously at low applied amplitudes in order to avoid undesirable electrochemical reactions and electrolysis of cells [37].

In this study, we applied rectangular AC electric pulses with adjustable V_a of 0–4 V, t_p of 0–8 ms and P_n of 1–10 on NSP-EP chips with different enhancement factor α (5.87, 7.55 and 8.95) to study EP at reduced voltages. Cell permeabilization was detected through the digital fluorescence microscopy. The η_{EP} were quantified by dual AO/PI fluorescent staining (Fig. 5(a)) while the ϕ_{cell} were quantified by dual AO/EB fluorescent staining (Fig. 5(b)).

Fluorescence micrographs before EP have no red fluorescence due to impermeability of cell membrane to PI dye molecules (Fig. 5(aII)). After the application of the electric pulses above a critical value, cell membrane became permeable due to the expansion of nano-pores on cell membranes by an electric field. PI molecules entered the cells through expanded nano-pores and bound with DNA/RNA. Electroporated cells exhibited red fluorescence while the non-electroporated cells exhibited green fluorescence (Fig. 5(aIII)). The fluorescence intensity increased quickly in first few minutes due to fast diffusion of PI dye molecules into the cells through the expanded nano-pores. After 3–4 min, the fluorescence reached a saturated value as the concentration of PI dye molecules achieved equilibrium state (see SI, Fig. S2).

The EP process can be divided into three phases (Fig. 4(b)). When applied electric field was smaller than the critical value E_{EP}; the electric field was unable to induce enough nanopores on the cell membrane. No noticeable change in fluorescence intensity was observed at this stage (see SI, Fig. S3(a)) and η_{EP} is very low at this stage. When applied electric field is above critical value E_{EP}, the electric field is strong enough to induce nanopores on cell membranes, and PI molecules can enter the cell through these pores. More and more cells exhibited stronger fluorescence with small increase in applied pulse amplitude V_a (see SI, Fig. S3(b)-(c)). The η_{EP} increased with large slope in this phase (Fig. 4b). The final stage was the saturation of fluorescence intensity; η_{EP} reached its maximum value. Further increase of pulse amplitude V_a, resulted in a decrease of cell viabilities.

3.6. Critical electric field for EP

From the above analysis, it is clear that there is critical value of the electric field for EP, E_{EP}, above which η_{EP} increased with large slope due to the influx of molecules into the cells through induced nano-pores. E_{EP} is different for different pulse duration t_P that is smaller for longer t_P and larger for shorter t_P (see SI, Fig. S4). For specific t_P, E_{EP} can be defined as the electric field corresponding to the onset of the increasing slope of the EP efficiency curve [30,64]. The E_{EP} has been achieved at V_a >10 V on a PEP device (Fig. 4(d)). As stated before, localized electric field E_{ns} increases with increasing α which implies that any specific electric field can be achieved at reduced voltages with increasingα. E_{EP} has been made at much lower voltages at higher α. For the NSP-EP chip with α of 5.87, E_{EP} has been accomplished at V_a = 3 V (Fig. 4(a)). Similarly for α of 7.55, E_{EP} has been reached at V_a = 2.3 V (Fig. 4(b)) and for α of 8.95, V_a has been reduced to ~1 V (Fig. 4(c)). E_{EP} has been achieved at 4–13

times lower voltages on NSP-EP chips with different α as compared to PEP devices.

3.7. Effect of enhancement factor on NSP-EP chip performance

Although the EP efficiency η_{EP} increases by increasing the electric field enhancement factorα, the cell viability Φ_{cell} decreases at higher α (Fig. 4). If α is too small, Φ_{cell} is high but η_{EP} is lower than 80% (Fig. 4(a)). If α is too high, η_{EP} is also high but Φ_{cell} is low due to very high localized electric field (Fig. 4(c)). So an optimized value of α should be selected and selection of α depends upon application. For example, NSPs with higher α values can be chosen for applications where high Φ_{cell} are not required or for electric cell lysis applications [65]. For applications where high η_{EP} and Φ_{cell} are required, NSPs with medium α can be selected. NSPs with α of 7.55 showed higher η_{EP} and Φ_{cell} simultaneously as compared to NSP-EP chips with other α and PEP devices (Fig. 4). EP experimental results demonstrated that EP on NSP-EP chips can be achieved at five times reduced voltages with high η_{EP} and Φ_{cell} as compared to the PEP device for single pulse (Fig. 4(d)). Bubble generation was observed on PEP devices due to high voltage operation, and this was avoided on NSP-EP chip due to low voltage operation. NSPs with α of 7.55 were selected as it provided higher η_{EP} and Φ_{cell} simultaneously for further studies in following sections.

3.8. Effect of electric pulse parameters on NSP-EP chip performance

The η_{EP} and Φ_{cell} are highly influenced by electric pulse parameters, such as V_a, t_P and P_n. Higher pulse amplitude V_a, longer pulse duration t_p and higher pulse number P_n resulted in higher permeability, hence higher η_{EP}. But cell viabilities Φ_{cell} decreased with higher V_a, longer t_p and higher P_n with increased permeabilities (see SI, Fig. S4-S5). There is a tradeoff between η_{EP} and Φ_{cell} and selection of electric pulse parameters depends on the biological application of interest. An optimized value of electric pulse parameters should be selected for high η_{EP} and Φ_{cell} simultaneously for efficient EP. For single pulse of 2 ms, 4 V was chosen as the optimal value at which high η_{EP} and Φ_{cell} was achieved (Fig. 4(b)).

It was observed that η_{EP} increased by increasing t_P and P_n and Φ_{cell} dropped more quickly by increasing t_P as compared to increasing P_n (see SI, Fig. S4-S5). At same pulse amplitude and pulse duration, higher η_{EP} were achieved with increasing P_n. For t_p of 2 ms and V_a of 2 V, η_{EP} was 56% for P_n of 1 and η_{EP} increased to 91% for P_n of 10 with same applied t_p and V_a (see SI, Fig. S5). In addition, a specific η_{EP} was achieved at lower voltages by increasing pulse number P_n. η_{EP} of >90% was achieved at 4 V for P_n = 1 and η_{EP} of >90% were achieved at 2 V for P_n = 10 that is half the applied amplitude for P_n = 1 (see SI, Fig. S5). High η_{EP} (> 93 ± 5%) was achieved at NSP-EP chips (α = 7.55) at low V_a of 2 V, t_p of 2 ms and P_n of 9 as compare to PEP devices at which η_{EP} was almost zero at V_a of 5 V (Fig. 5(a)). Besides, high Φ_{cell} (> 93 ± 6%) was achieved at NSP-EP chips (α = 7.55) at low V_a of 2 V, t_p of 2 ms and P_n of 9 as compare to PEP devices (Fig. 5(b)). At PEP devices, η_{EP} was ~0% at V_a of 10 V while Φ_{cell} was around 89% (Fig. 5(c)). By optimizing electric pulse parameters, we are able to achieve high η_{EP} and Φ_{cell} (> 93 ± 6%) at low V_a of 2 V and t_p of 2 ms for P_n of 9 and 10 at NSP-EP chips (α = 7.55) (Fig. 5(c)).

3.9. Undesirable electrochemical reactions

We performed electroporation of HeLa cells on PEP device and NSP-EP chips with same device dimensions and interelectrode distance. η_{EP} and Φ_{cell} were determined after application of different electric pulse parameters. The critical electric field for EP values for PEP and NSP-EP chip were determined from η_{EP} and Φ_{cell} curves. For NSP-EP chips, high η_{EP} and Φ_{cell} (>93 ± 6%) were achieved at low applied amplitudes (2 V) while for PEP device at 10 V; η_{EP} was ~0% (Fig. 4(d)). E_{EP} has been achieved at V_a >10 V on a PEP device (Fig. 4(d)). Due to the NSP's enhanced electric field, E_{EP} has been achieved at V_a = 2.3 V for t_p of 2 ms and P_n of 1 on an NSP-EP chip (α = 7.55) (Fig. 4(d)). E_{EP} has been achieved on a NSP-EP chip (α = 7.55) at V_a = 0.8 V for P_n of 10 and for t_p of 6 ms and above. This is five to twenty times lower as compared to the PEP device (Fig. 6).

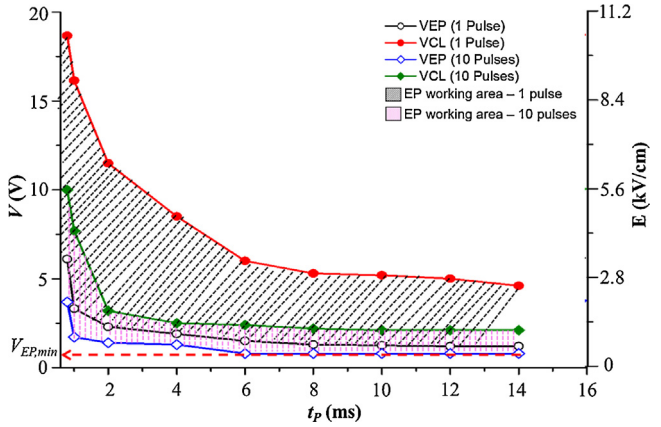

Fig. 6. The phase diagram for EP and electric cell lysis of HeLa cells on NSP-EP chips with α = 7.5 for 1 and 10 pulses. Phase diagram shows the critical electric field strength and voltages for EP (E_{EP}, V_{EP}) and electric cell lysis (E_{CL}, V_{CL}) on NSP-EP chip for different pulse duration and number. Minimum V_{EP} ($V_{EP,min}$) is obtained at 0.8 V with P_n of 10 and t_p of 6 ms or above.

Relatively high voltage (few tens of volts) in macro and micro EP devices resulted in low reliability and device failure due to joule heating, electrolysis, gas bubble generation, local pH variations, etc [60]. Cells were found damaged and lysed during EP process due to gas bubbles generation which resulted in local pH variations and violent hydrodynamic forces due to bubble generation or collapse process [30,60]. Gas bubble generation was observed on PEP device when high voltages (> 10 V) are applied to achieve high η_{EP} but Φ_{cell} dropped. These applied voltages were high enough for severe electrochemical reactions which resulted in bubble generation and electrode degradation. On NSP-EP chips, due to low voltage operation; high η_{EP} and Φ_{cell} (> 90%) were achieved without bubble generation.

3.10. Phase diagram

Electroporation is a threshold phenomenon; EP occurs successfully when V_a, t_p and P_n are well above a critical value. But if these values are too high, the cell will undergo an irreversible process and will be unable to reseal and repair changes and lysed. It is very important to define the boundary for non-EP, EP, electric cell lysis regions. The critical electric field strength for EP (E_{EP}) for the pulse duration is defined as the electric field strength at the onset of increasing slope of the EP efficiency curve for that pulse duration. The E_{EP} for suspended HeLa cells for single electric pulse is 1.6 kV/cm (2.3 V) for 2 ms, 1.3 kV/cm (1.9 V) for 4 ms, 1.16 kV/cm (1.5 V) for 6 ms, and 1.03 kV/cm (1.3 V) for 8 ms (see SI, Fig. S4). These critical values were even lower at higher pulse number for specific pulse duration (see SI, Fig. S5). Critical electric field strength for electric cell lysis (E_{CL}) is also defined to set the boundary between EP and cell lysis regions.

Experiments were carried out on NSP-EP chips (α = 7.55) and V_{EP}, E_{EP}, V_{CL} and E_{CL} were determined for different pulse widths (t_P) and pulse number (P_n). These values were used to construct "phase diagram" for EP of HeLa cells on NSP-EP chips (Fig. 6). Phase diagram defines the boundary for the non-EP region, EP region and electric cell lysis region based on E_{EP} and E_{CL} at different t_P

and P_n. Phase diagram can be used for the optimization of electrical parameters for efficient EP with reasonable cell viabilities. Clearly, E_{EP} was achieved at lower voltages by increasing t_P and even ultra-low voltages by increasing P_n. Minimum V_{EP} ($V_{EP,min}$) is obtained at 0.8 V with P_n of 10 and t_P of 6 ms or above. The low-voltage NSP-EP chips are highly attractive for the integration of the other μ-TAS functions, such as electric cell lysing, electrical detection of biomolecules and cancer cells [60,62,65]. Based on these low voltage NSP-EP devices, we recently developed "Smartphone-based Electroporator system" in which optimized EP protocols for different types of cells and molecules in a control app of an Android smartphone can be applied to micro/nano EP chips through an open-source MCU (Arduino) with an integrated Bluetooth module [49].

4. Conclusions

In this paper, we present a highly ordered 3D scalable nano-spike electroporation platform for efficient intracellular delivery with high cell viabilities at low pulse amplitude and duration, which minimized undesirable electrochemical reactions and electrolysis significantly and increase the device's reliability and cell viabilities. Highly ordered 3D nano-spikes arrays were fabricated with controllable geometries using simple, scalable, reproducible and cost-effective electrochemical anodization and etching processes. Due to scalability of the fabrication process, 3D NSPs were fabricated on chips for handling small populations as well as on wafer level for large scale processing. Electroporation at reduced voltages was observed due to electric field enhancement at high-aspect-ratio nano-spikes as compared to the PEP devices without nano-spikes. High EP efficiencies and cell viabilities (>93 ± 6%) were achieved at low voltages (2 V) on NSP-EP chips by optimizing electric pulse protocol and nano-spikes dimensions. This applied voltage is more than ten times lower as compared to PEP devices. Due to low voltage operation on NSP-EP chips; EP was carried out without bubble generation. Due to high voltage operation on planar electroporation (PEP) devices, bubble generation was observed. The EP phase diagram was constructed by determining critical electric fields for non-EP, EP and cell lysis for different electric pulse parameters. Minimum voltage required to generate a critical electric field to induce EP was obtained at 0.8 V for a pulse number of 10 and pulse duration of 6 ms or above. This is more than sixteen times lower as compared to PEP devices. Simple, low-cost and scalable fabrication process for high-aspect-ratio nano-spikes along with low voltage operation can enable the integration of digital miniaturized electroporator to μ-TAS, LOC and smartphone systems.

Acknowledgements

This research was supported by a grant from the Hong Kong Research Grants Council (Ref No. 16205314).

Appendix A. Supplementary data

Supplementary data associated with this article can be found, in the online version, at http://dx.doi.org/10.1016/j.sna.2016.12.022.

References

[1] M.L. Kovarik, D.M. Ornoff, A.T. Melvin, N.C. Dobes, Y. Wang, A.J. Dickinson, et al., Micro total analysis systems: fundamental advances and applications in the laboratory, clinic, and field, Anal. Chem. 85 (2013) 451–472, http://dx.doi.org/10.1021/ac3031543.
[2] N. Rajabi, J. Bahnemann, T.-N. Tzeng, O. Platas Barradas, A.-P. Zeng, J. Müller, Lab-on-a-chip for cell perturbation, lysis, and efficient separation of sub-cellular components in a continuous flow mode, Sens. Actuators A Phys. 215 (2014) 136–143, http://dx.doi.org/10.1016/j.sna.2013.12.019.
[3] H. Andersson, A. van den Berg, Microfluidic devices for cellomics: a review, Sens. Actuators B Chem. 92 (2003) 315–325, http://dx.doi.org/10.1016/S0925-4005(03)00266-1.
[4] Y.C. Lim, A.Z. Kouzani, W. Duan, Lab-on-a-chip: a component view, Microsyst. Technol. 16 (2010) 1995–2015, http://dx.doi.org/10.1007/s00542-010-1141-6.
[5] D. Luo, W.M. Saltzman, Synthetic DNA delivery systems, Nat. Biotechnol. 18 (2000) 33–37, http://dx.doi.org/10.1038/71889.
[6] D.J. Stephens, R. Pepperkok, The many ways to cross the plasma membrane, Proc. Natl. Acad. Sci. U. S. A. 98 (2001) 4295–4298, http://dx.doi.org/10.1073/pnas.081065198.
[7] T.K. Kim, J.H. Eberwine, Mammalian cell transfection: the present and the future, Anal. Bioanal. Chem. 397 (2010) 3173–3178, http://dx.doi.org/10.1007/s00216-010-3821-6.
[8] S. Mehier-Humbert, R.H. Guy, Physical methods for gene transfer: improving the kinetics of gene delivery into cells, Adv. Drug Deliv. Rev. 57 (2005) 733–753, http://dx.doi.org/10.1016/j.addr.2004.12.007.
[9] J.C. Weaver, Electroporation of cells and tissues, IEEE Trans. Plasma Sci. 28 (2000) 24–33, http://dx.doi.org/10.1109/27.842820.
[10] J. Gehl, Electroporation: theory and methods, perspectives for drug delivery, gene therapy and research, Acta Physiol. Scand. 177 (2003) 437–447, http://dx.doi.org/10.1046/j.1365-201X.2003.01093.x.
[11] N. Odani, K. Ito, H. Nakamura, Electroporation as an efficient method of gene transfer, Dev. Growth Differ. 50 (2008) 443–448, http://dx.doi.org/10.1111/j.1440-169X.2008.01037.x.
[12] W.G. Lee, U. Demirci, A. Khademhosseini, Microscale electroporation: challenges and perspectives for clinical applications, Integr. Biol. (Camb) 1 (2009) 242–251, http://dx.doi.org/10.1039/b819201d.
[13] J.A. Kim, K. Cho, M.S. Shin, W.G. Lee, N. Jung, C. Chung, et al., A novel electroporation method using a capillary and wire-type electrode, Biosens. Bioelectron. 23 (2008) 1353–1360, http://dx.doi.org/10.1016/j.bios.2007.12.009.
[14] T. Geng, C. Lu, Microfluidic electroporation for cellular analysis and delivery, Lab Chip. 13 (2013) 3803–3821, http://dx.doi.org/10.1039/c3lc50566a.
[15] S. Movahed, D. Li, Microfluidics cell electroporation, Microfluid. Nanofluidi. 10 (2010) 703–734, http://dx.doi.org/10.1007/s10404-010-0716-y.
[16] M. Puc, S. Corović, K. Flisar, M. Petkovsek, J. Nastran, D. Miklavcic, Techniques of signal generation required for electropermeabilization. Survey of electropermeabilization devices, Bioelectrochemistry 64 (2004) 113–124, http://dx.doi.org/10.1016/j.bioelechem.2004.04.001.
[17] Y. Huang, B. Rubinsky, Flow-through micro-electroporation chip for high efficiency single-cell genetic manipulation, Sens. Actuators A Phys. 104 (2003) 205–212, http://dx.doi.org/10.1016/S0924-4247(03)00050-5.
[18] Y.-C. Lin, M. Li, C.-S. Fan, L.-W. Wu, A microchip for electroporation of primary endothelial cells, Sens. Actuators A Phys. 108 (2003) 12–19, http://dx.doi.org/10.1016/j.sna.2003.05.002.
[19] Y. Huang, B. Rubinsky, Microfabricated electroporation chip for single cell membrane permeabilization, Sens. Actuators A Phys. 89 (2001) 242–249, http://dx.doi.org/10.1016/S0924-4247(00)00557-4.
[20] N. Wilke, C. Hibert, J. O'Brien, A. Morrissey, Silicon microneedle electrode array with temperature monitoring for electroporation, Sens. Actuators A Phys. 123-124 (2005) 319–325, http://dx.doi.org/10.1016/j.sna.2005.05.017.
[21] B.I. Morshed, M. Shams, T. Mussivand, Investigation of low-voltage pulse parameters on electroporation and electrical lysis using a microfluidic device with interdigitated electrodes, IEEE Trans. Biomed. Eng. 61 (2014) 871–882, http://dx.doi.org/10.1109/tbme.2013.2291794.
[22] H. He, D.C. Chang, Y.-K. Lee, Using a micro electroporation chip to determine the optimal physical parameters in the uptake of biomolecules in HeLa cells, Bioelectrochemistry 70 (2007) 363–368, http://dx.doi.org/10.1016/j.bioelechem.2006.05.008.
[23] S. Wang, X. Zhang, W. Wang, L.J. Lee, Semicontinuous flow electroporation chip for high-throughput transfection on mammalian cells, Anal. Chem. 81 (2009) 4414–4421, http://dx.doi.org/10.1021/ac9002672.
[24] R.A. Lawes, Manufacturing costs for microsystems/MEMS using high aspect ratio microfabrication techniques, Microsyst. Technol. 13 (2006) 85–95, http://dx.doi.org/10.1007/s00542-006-0252-6.
[25] W. Ebina, A.C. Rowat, D.A. Weitz, Electrodes on a budget: micropatterned electrode fabrication by wet chemical deposition, Biomicrofluidics 3 (2009) 34104, http://dx.doi.org/10.1063/1.3224669.
[26] G.D. Troszak, B. Rubinsky, A primary current distribution model of a novel micro-electroporation channel configuration, Biomed. Microdevices 12 (2010) 833–840, http://dx.doi.org/10.1007/s10544-010-9437-y.
[27] M.B. Fox, D.C. Esveld, A. Valero, R. Luttge, H.C. Mastwijk, P.V. Bartels, et al., Electroporation of cells in microfluidic devices: a review, Anal. Bioanal. Chem. 385 (2006) 474–485, http://dx.doi.org/10.1007/s00216-006-0327-3.
[28] R. Stapulionis, Electric pulse-induced precipitation of biological macromolecules in electroporation, Bioelectrochem. Bioenerg. 48 (1999) 249–254, http://dx.doi.org/10.1016/S0302-4598(98)00206-2.
[29] J.W. Loomis-Husselbee, P.J. Cullen, R.F. Irvine, A.P. Dawson, Electroporation can cause artefacts due to solubilization of cations from the electrode plates. Aluminum ions enhance conversion of inositol 1,3,4,5-tetrakisphosphate into inositol 1,4,5-trisphosphate in electroporated L1210 cells, Biochem. J. 277 (Pt 3) (1991) 883–885, http://www.ubmedcentral.nih.gov/articlerender.fcgi?artid=1151327&tool=mcentrez&rendertye=abstract (Accessed 17 December 2015).

[30] P. Deng, D.C. Chang, Y.-K. Lee, J. Zhou, G. Li, DNA transfection of bone marrow mesenchymal stem cells using micro electroporation chips, in: 2011 6th IEEE International Conference on Nano/Micro Engineered and Molecular Systems, IEEE, 2011, pp. 96–99, http://dx.doi.org/10.1109/NEMS. 2011.6017304.
[31] H.-Y. Wang, C. Lu, Electroporation of mammalian cells in a microfluidic channel with geometric variation, Anal. Chem. 78 (2006) 5158–5164, http://dx.doi.org/10.1021/ac060733n.
[32] Jinpeng Wang, Shih-Chi Yang, Cheng Wang, Qiong Wu, Zheyao Wang, A DEP-assisted single-cell electroporation chip with low operation voltage, in: 2010 IEEE Sensors, IEEE, 2010, http://dx.doi.org/10.1109/ICSENS.2010.5690354.
[33] H. Shintaku, K. Hakamada, H. Fujimoto, T. Nagata, J. Miyake, S. Kawano, Measurement of local electric field in microdevices for low-voltage electroporation of adherent cells, Microsyst. Technol. 20 (2013) 303–313, http://dx.doi.org/10.1007/s00542-013-1797-9.
[34] R. Ziv, Y. Steinhardt, G. Pelled, D. Gazit, B. Rubinsky, Micro-electroporation of mesenchymal stem cells with alternating electrical current pulses, Biomed. Microdevices 11 (2009) 95–101, http://dx.doi.org/10.1007/s10544-008-9213-4.
[35] J.H. Sung, M.L. Shuler, Prevention of air bubble formation in a microfluidic perfusion cell culture system using a microscale bubble trap, Biomed. Microdevices 11 (2009) 731–738, http://dx.doi.org/10.1007/s10544-009-9286-8.
[36] T. Kotnik, D. Miklavčič, L.M. Mir, Cell membrane electropermeabilization by symmetrical bipolar rectangular pulses, Bioelectrochemistry 54 (2001) 91–95, http://dx.doi.org/10.1016/S1567-5394(01)00115-3.
[37] K. Riaz, S.-F. Leung, H. Shagoshtasbi, Z. Fan, Y.-K. Lee, Optimization of multiple-pulse ultra-low voltage Nanospike electroporation chips using feedback system control for efficient delivery of molecules to cancer cells, in: 10th IEEE International Conference on Nano/Micro Engineered and Molecular Systems, IEEE, 2015, pp. 263–267, http://dx.doi.org/10.1109/NEMS. 2015.7147423.
[38] S. Wang, L.J. Lee, Micro-/nanofluidics based cell electroporation, Biomicrofluidics 7 (2013) 11301, http://dx.doi.org/10.1063/1.4774071.
[39] J.A. Rojas-Chapana, M.A. Correa-Duarte, Z. Ren, K. Kempa, M. Giersig, Enhanced introduction of gold nanoparticles into vital acidothiobacillus ferrooxidans by carbon nanotube-based microwave electroporation, Nano Lett. 4 (2004) 985–988, http://dx.doi.org/10.1021/nl049699n.
[40] V. Raffa, G. Ciofani, A. Cuschieri, Enhanced low voltage cell electropermeabilization by boron nitride nanotubes, Nanotechnology 20 (2009) 075104, http://dx.doi.org/10.1088/0957-4484/20/7/075104.
[41] V. Raffa, G. Ciofani, O. Vittorio, V. Pensabene, A. Cuschieri, Carbon nanotube-enhanced cell electropermeabilisation, Bioelectrochemistry 79 (2010) 136–141, http://dx.doi.org/10.1016/j.bioelechem.2009.10.006.
[42] Carbon Nanotubes for Voltage Reduction and Throughput Enhancement of Electrical Cell Lysis on a Lab-on-a-chip – Metrics – Nanotechnology – IOPscience, 2011, http://m.iopscience.iop.org/0957-4484/22/32/325705/metrics (Accessed 2 June 2015).
[43] S.-C. Chen, T.S. Santra, C.-J. Chang, T.-J. Chen, P.-C. Wang, F.-G. Tseng, Delivery of molecules into cells using localized single cell electroporation on ITO micro-electrode based transparent chip, Biomed. Microdevices. 14 (2012) 811–817, http://dx.doi.org/10.1007/s10544-012-9660-9.
[44] T.S. Santra, P.-C. Wang, H.-Y. Chang, F.-G. Tseng, Tuning nano electric field to affect restrictive membrane area on localized single cell nano-electroporation, Appl. Phys. Lett 103 (2013) 233701, http://dx.doi.org/10.1063/1.4833535.
[45] N. Jokilaakso, E. Salm, A. Chen, L. Millet, C.D. Guevara, B. Dorvel, et al., Ultra-localized single cell electroporation using silicon nanowires, Lab Chip. 13 (2013) 336–339, http://dx.doi.org/10.1039/c2lc40837f.
[46] X. Xie, A.M. Xu, S. Leal-Ortiz, Y. Cao, C.C. Garner, N.A. Melosh, Nanostraw-electroporation system for highly efficient intracellular delivery and transfection, ACS Nano 7 (2013) 4351–4358, http://dx.doi.org/10.1021/nn400874a.
[47] M. Shahini, J.T.W. Yeow, Cell electroporation by CNT-featured microfluidic chip, Lab Chip. 13 (2013) 2585–2590, http://dx.doi.org/10.1039/c3lc00014a.
[48] P.E. Boukany, A. Morss, W.-C. Liao, B. Henslee, H. Jung, X. Zhang, et al., Nanochannel electroporation delivers precise amounts of biomolecules into living cells, Nat. Nanotechnol. 6 (2011) 747–754, http://dx.doi.org/10.1038/nnano.2011.164.
[49] H. Shagoshtasbi, K. Riaz, Y.-K. Lee, K. Tse, Smartphone-based electroporator system for micro/nano electroporation chips, in: 10th IEEE International Conference on Nano/Micro Engineered and Molecular Systems, IEEE, 2015, pp. 72–75, http://dx.doi.org/10.1109/NEMS. 2015.7147376.
[50] A. Santos, M.J. Deen, L.F. Marsal, Low-cost fabrication technologies for nanostructures: state-of-the-art and potential, Nanotechnology 26 (2015) 042001, http://dx.doi.org/10.1088/0957-4484/26/4/042001.
[51] G.E.J. Poinern, N. Ali, D. Fawcett, Progress in nano-Engineered anodic aluminum oxide membrane development, Materials (Basel) 4 (2011) 487–526, http://dx.doi.org/10.3390/ma4030487.
[52] R. Yu, K.-L. Ching, Q. Lin, S.-F. Leung, D. Arcrossito, Z. Fan, Strong light absorption of self-organized 3-D nanospike arrays for photovoltaic applications, ACS Nano 5 (2011) 9291–9298, http://dx.doi.org/10.1021/nn203844z.
[53] Y. Qiu, S.-F. Leung, Q. Zhang, B. Hua, Q. Lin, Z. Wei, et al., Efficient photoelectrochemical water splitting with ultrathin films of hematite on three-dimensional nanophotonic structures, Nano Lett. 14 (2014) 2123–2129, http://dx.doi.org/10.1021/nl500359e.
[54] S.-F. Leung, K.-H. Tsui, Q. Lin, H. Huang, L. Lu, J.-M. Shieh, et al., Large scale, flexible and three-dimensional quasi-ordered aluminum nanospikes for thin film photovoltaics with omnidirectional light trapping and optimized electrical design, Energy Environ. Sci. 7 (2014) 3611–3616, http://dx.doi.org/10.1039/C4EE01850H.
[55] S.-F. Leung, L. Gu, Q. Zhang, K.-H. Tsui, J.-M. Shieh, C.-H. Shen, et al., Roll-to-roll fabrication of large scale and regular arrays of three-dimensional nanospikes for high efficiency and flexible photovoltaics, Sci. Rep. 4 (2014) 4243, http://dx.doi.org/10.1038/srep04243.
[56] M. Hamadouche, P. Boutin, J. Daussange, M.E. Bolander, L. Sedel, Alumina-on-alumina total hip arthroplasty: a minimum 18.5-year follow-up study, J. Bone Joint Surg. Am. 84-A (2002) 69–77, http://jbjs.org/content/84/1/69.abstract (Accessed 20 December 2015).
[57] L.G. Parkinson, N.L. Giles, K.F. Adcroft, M.W. Fear, F.M. Wood, G.E. Poinern, The potential of nanoporous anodic aluminium oxide membranes to influence skin wound repair, Tissue Eng. Part A 15 (2009) 3753–3763, http://dx.doi.org/10.1089/ten.TEA.2008.0594.
[58] A.R. Walpole, E.P. Briggs, M. Karlsson, E. Pålsgård, P.R. Wilshaw, Nano-porous alumina coatings for improved bone implant interfaces, Materwiss Werksttech 34 (2003) 1064–1068, http://dx.doi.org/10.1002/mawe.200300707.
[59] A. Hoess, N. Teuscher, A. Thormann, H. Aurich, A. Heilmann, Cultivation of hepatoma cell line HepG2 on nanoporous aluminum oxide membranes, Acta Biomater. 3 (2007) 43–50, http://dx.doi.org/10.1016/j.actbio.2006.07.007.
[60] K. Riaz, S.-F. Leung, S. Tripathi, G.S. Sethi, H. Shagoshtasbi, Z. Fan, et al., An Aluminum Nano-Spike electroporation chip for low voltage delivery of molecules to cancer cells, in: 9th IEEE International Conference on Nano/Micro Engineered and Molecular Systems, IEEE, 2014, pp. 147–151, http://dx.doi.org/10.1109/NEMS. 2014.6908779.
[61] R.G. Forbes, C. Edgcombe, U. Valdrè, Some comments on models for field enhancement, Ultramicroscopy 95 (2003) 57–65, http://dx.doi.org/10.1016/S0304-3991(02)00297-8.
[62] K. Riaz, C. Zhao, T.S. Lau, S.F. Leung, Z. Fan, Y.K. Lee, Low-cost Nano-spike Bio-Impedance Sensor (NBIS) without surface functionalization for detection and phenotyping of cancer cells, in: 2015 Transducers – 2015 18th International Conference on Solid-State Sensors, Actuators Microsystems, IEEE, 2015, pp. 367–370, http://dx.doi.org/10.1109/TRANSDUCERS. 2015.7180937.
[63] H. He, D.C. Chang, Y.-K. Lee, Nonlinear current response of micro electroporation and resealing dynamics for human cancer cells, Bioelectrochemistry 72 (2008) 161–168, http://dx.doi.org/10.1016/j.bioelechem.2008.01.007.
[64] P. Deng, Y.-K. Lee, R. Lin, T.-Y. Zhang, Nonlinear electro-mechanobiological behavior of cell membrane during electroporation, Appl. Phys. Lett. 101 (2012) 053702, http://dx.doi.org/10.1063/1.4739940.
[65] K. Riaz, S.F. Leung, Z. Fan, Y.-K. Lee, Aluminum nano-Spike electric cell lysing with ultra-low applied voltages, 7th Asia-Pacific Conference Transducers Micro-Nanotechnology (APCOT 2014) (2014), http://repository.ust.hk/ir/Record/1783.1-69411 (Accessed 7 September 2015).

Biographies

Kashif Riaz obtained his BS degree in Electronic Engineering, Engineering in University College of Engineering and Technology, IUB, Pakistan. He obtained his MS degree in Elctronics Engineering, MEMS and Microsystems, Ghulam Ishaq Khan Institute of Information and Technology, Topi, N.W.F.P, Pakistan. He received his PhD student working on micro/nano electroporaton research at Hong Kong University of Science and Technology in 2016.

Siu-Fung Leung obtained his B.S. degree in Physics and Materials Science in the City University of Hong Kong. He pursued his PhD degree in Electronic and Computer Engineering, HKUST in 2015. He is currently a post doctoral researcher at HKUST.

Zhiyong Fan received his B.S. and M.S. degree in physical electronics from Fudan University, Shanghai, China, in 1998 and 2001. He received Ph.D. degree from University of California, Irvine in 2006 in Materials Science. From 2007–2010, he worked in University of California, Berkeley as a postdoctoral fellow in department of Electrical Engineering and Computer Sciences, with a joint appointment with Lawrence Berkeley National Laboratory. In May 2010, he joined the faculty of Hong Kong University of Science and Technology and currently he is an associate professor at Department of Electronic and Computer Engineering. He currently serves as an editorial board member of NPG Scientific Reports and Associate Editor of Springer Nanoscale Research Letters. He also serves as a peer reviewer for Nature Materials, Nature Nanotechnology, Nature Communications, Nano Letters, ACS Nano, Advanced Materials, Energy &Environmental Science, Angewandte Chemie, IEEE EDL, etc. His research focuses on novel functional nanomaterials and their applications in energy conversion, nanoelectronics, gas sensing and biomedical engineering. He has remarkable achievements in novel types of nanowire synthesis and cutting-edge technologies, such as wafer scale nanowire assembly for gas sensing and Nanoelectronics applications.

Yi-Kuen Lee received his B.S. degree with honor in Biomechatronic Industrial Engineering Department, National Taiwan University (NTU) and his M.S. degree in applied mechanics, NTU. He obtained his PhD degree in MEMS at UCLA in 2001. He has been actively working in the design and fabrication of MEMS/NEMS and

microfluidics devices for DNA dynamic study, DNA hybridization enhancement, DNA microarray printing, DNA separation, micro electroporation chips, CMOS MEMS flow sensors, etc. A silicon-based microfluidic chip was fabricated to study single DNA molecule dynamics in microchannels. A series of electrokinetic microfluidic devices were constructed for micro mixing, vortex generation and flow control. He also investigated the influence of different concentrations of single-stranded DNA on bubble dynamics, which has promising application in the enhancement of DNA hybridization. In addition, a novel free-solution electrophoresis microsystem integrated with driving electrodes and sub-micron pillar arrays was fabricated and characterized using a mixture of large DNA molecues (T4 DNA and lambda DNA). The geometry of the pillar array could dramatically change the electrophoretic mobility of the DNA molecules.